# Controlled Introduction of Metal Nanoparticles into a Microdomain Structure

**Satoshi Akasaka, Hiroki Mori, Taketsugu Osaka, Vincent H. Mareau, and Hirokazu Hasegawa***

*Department of Polymer Chemistry, Graduate School of Engineering, Kyoto University, Kyoto 615-8510, Japan*

*Received August 6, 2008; Revised Manuscript Received January 8, 2009*

ABSTRACT: We successfully developed a method to control the introduction of Pd nanoparticles selectively into the poly(2-vinylpyridine) (P2VP) microdomains of polyisoprene-*block*-poly(2-vinylpyridine) (PI-*b*-P2VP) diblock copolymer. The technique consists of three steps: (i) cross-linking of P2VP microdomains with diiodobutane (DIB), (ii) immersion of the cross-linked film in the mixture of palladium diacetate ($Pd(acac)_2$), benzyl alcohol, and toluene, and (iii) annealing the immersed and dried film at 230 °C for 30 min. With this method, we could generate Pd nanoparticles with considerably uniform size (5.5 nm) by *in situ* reduction of the Pd ions solely within the P2VP microdomains without disturbing the regular microdomain structure of PI-*b*-P2VP diblock copolymer. We employed 3D electron tomography to analyze the location and the size of the Pd nanoparticles and demonstrated its capability in the analysis of nanoparticle/block copolymer systems.

## 1. Introduction

In the recent decade there has been a great deal of interest in creating functional structures in nanometer scale using block copolymer microdomain structures. When the conventional block copolymers are used to prepare functional materials, it is necessary to introduce some functional materials, which can add some useful functionalities to the block copolymers when they themselves do not have desirable functionalities.

Metal nanoparticles of less than ten nanometers in diameter have different properties and functionalities from their bulk due to the quantum size effect.[1−3] Therefore, metal nanoparticles are good candidates to be added to the block copolymer. However, metal nanoparticles are not stable by themselves and strongly tend to aggregate into large clusters. To create advanced functional materials having superior optic, electronic, magnetic, thermal, or catalytic properties with metal nanoparticles, their surfaces should be protected with some ligands or polymers against aggregation.[4−6] Furthermore, it is important to align the metal nanoparticles in a regular array with a template to enhance their featuring properties.[7−9]

It is well-known that diblock copolymers form ordered nanometer-scale microdomain structures such as bcc spheres, hexagonally packed cylinders, bicontinuous double-networks, and lamellae. Morphology and domain sizes of diblock copolymers can be readily controlled by changing their compositions and molecular weights.[10−15] Besides, since their domain sizes are in the range of 10−100 nm, block copolymers are suitable for a template to align or a supporting material of the metal nanoparticles.

Many works on introduction of nanoparticles into block copolymers have been reported so far.[16−46] There are basically two different techniques. One is mixing surface-modified metal nanoparticles with block copolymers by solution blending. The other is generating metal nanoparticles *in situ* in block copolymers. To give an example of the former case, Bockstaller et al.[34] achieved a highly selective introduction of the surface-modified Au and $SiO_2$ nanoparticles with different core sizes into different locations of the micorodomains of polystyrene-*block*-poly(ethylene-*co*-propylene) diblock copolymer (PS-*b*-PEP) by blending the block copolymer with the nanoparticles. They blended two different nanoparticles, Au and $SiO_2$, having two distinct diameters at once with the block copolymer in solution and demonstrated that they could control the locations of the nanoparticles by adjusting the particle core sizes. The particles with the smaller core size (Au) were found predominantly near the interfaces of the lamellar domains, and the others with the larger core size ($SiO_2$) were localized near the center of the PEP domains. The limitation of this technique is that the amount of nanoparticles introduced in the microdomains is limited relatively low because blending an excess amount of nanoparticles results in precipitation of the nanoparticles and/or destruction of the regular microdomain structures of the block copolymers.

As for an example of the latter case, Hashimoto et al.[18] reported selective introduction of Pd nanoparticles into P2VP domains of polyisoprene-*block*-poly(2-vinylpyridine) diblock copolymer (PI-*b*-P2VP). They first prepared the film sample by casting PI-*b*-P2VP from solution in a mixture of toluene, palladium diacetate ($Pd(acac)_2$) and benzyl alcohol, and then annealed the film. The Pd ion (Pd(II)) and the alcohol, which is less volatile (bp = 204.7 °C), remained in the film even after the evaporation of toluene. The Pd ion was reduced by benzyl alcohol to generate Pd nanoparticles on subsequent annealing at 140 °C. They found the Pd nanoparticles predominantly in the P2VP domains of the PI-*b*-P2VP film. The adavantage of this technique is that a large quantity of Pd nanoparticles can be introduced into the P2VP domains of the PI-*b*-P2VP though the selectivity reduces with increasing the amount of nanoparticles. The excess introduction of Pd nanoparticles often results in loss of microdomain regularity. Another limitation of this technique is that the addition of benzyl alcohol might change the microdomain morphology because it is not a neutral solvent for PI and P2VP.

Adachi et al.[23] investigated in situ reduction of $Pd(acac)_2$ and introduction of Pd nanoparticles into a P2VP network texture. They first cross-linked the P2VP microdomains of a PI-*b*-P2VP film having gyroid morphology with 1,4-diiodobutane (DIB), removed the PI microdomains selectively by ozonolysis, and generated Pd nanoparticles in situ in the film by placing it in a 1-propanol/toluene/$Pd(acac)_2$ bath at 85 °C. They found the Pd nanoparticles introduced into the P2VP networks. They observed

* To whom correspondence should be addressed. E-mail: hasegawa@alloy.polym.kyoto-u.ac.jp.

10.1021/ma802674k CCC: $40.75 
Published on Web 02/03/2009

that the size of the Pd nanoparticles increased with the reduction time $t$ following the power law of $t^{-1/6}$ in agreement with a diffusion and coalescence model without hydrodynamic interactions. Jnnai et al.[47] investigated the location of the Pd nanoparticles in the P2VP network texture prepared by the same technique in 3D using electron tomography. They found that the Pd nanoparticles only at the surfaces of the P2VP networks. Therefore, the location of the introduced Pd nanoparticles could depend on the preparation conditions. Another disadvantage of this technique is that the reduction of Pd ion occurs also in the solution resulting in the waste of Pd ion.

In the case of block copolymer thin films having 2D nanopatterns, uniform introduction of metal nanoparticles into particular microdomains is not so complicated because it is less important to consider the particle distribution along the thickness direction of the thin films. However, in the case of thick films, uniform introduction of metal nanoparticles along the thickness direction is not so easy. Nonuniform biased distribution of nanoparticles in the thickness direction of the films is often resulted.[48,49] Therefore, it is necessary to develop a technique to control uniform distribution of nanoparticles in the thickness direction of the films.

In this paper, we report an excellent technique for selective introduction of metal nanoparticles into a thick block copolymer film. We could achieve (i) extremely high selectivity in introduction of nanoparticles into the microdomains of a particular component of a block copolymer, (ii) uniform particle size, (iii) control of the amount of nanoparticles introduced in the microdomains, (iv) uniform distribution of nanoparticles within the thickness of the film, (v) no destruction of original regular microdomain structure, and (vi) no waste of precursor material for metal nanoparticles at the same time.

Diblock copolymers having P2VP as one component are especially interesting because of the strong interaction of P2VP with metal nanoparticles. We chose PI-*b*-P2VP as the block copolymer and Pd as the metal nanoparticles and employed *in situ* reduction of Pd ion. In the process to achieve such control, we clarified the factors responsible for each process. We also employed a novel technique, 3D electron tomography,[47,50−53] to evaluate the distributions in size and locations of Pd nanoparticles in the PI-*b*-P2VP microdomains. Consequently, we could demonstrate the importance of particle analysis in three-dimensional real space.

## 2. Experimental Section

**2.1. Film Preparation.** We used PI-*b*-P2VP diblock copolymer with the number-average molecular weight $M_n = 40.7$ kg/mol, the polydispersity index $M_w/M_n = 1.03$ and the composition PI/P2VP = 49.6/50.4 (wt %/wt %) (Polymer Source, Inc.). We prepared a 0.5 mm thick PI-*b*-P2VP film by casting from 5 wt % solution in toluene by slow evaporation of solvent for 1 week at room temperature.

**2.2. Cross-Linking.** We used DIB to selectively cross-link the P2VP domains. The as-cast film was exposed to DIB vapor at 85 °C for 24 h resulting in the insoluble film in toluene. After cross-linking, the P2VP domains have a dark contrast in TEM observation due to the iodine atoms of the DIB cross-linking the P2VP chains.

**2.3. Reduction Methods of Metal Nanoparticles.** We tried three methods for introduction of nanoparticles into the microdomain structure of PI-*b*-P2VP.

*2.3.1. Method 1.* In method 1, the polymer films after cross-linking were immersed in a mixture of 150 mg of $Pd(acac)_2$ (Aldrich), 5 mL of benzyl alcohol, and 30 mL of toluene at 85 °C for 1 day. Subsequently, the films were dried in the ambient atmosphere for 1 day, and then annealed at 230 °C for 30 min under vacuum.

*2.3.2. Method 2.* In method 2, the polymer films after cross-linking were immersed in a mixture of 150 mg of $Pd(acac)_2$ and 30 mL of toluene at 30 or 85 °C for 1 day. Subsequently, the films were dried in the ambient atmosphere for 1 day, and then annealed at 230 °C for 30 min under vacuum.

*2.3.3. Method 3.* In method 3, the polymer films after cross-linking were immersed in a mixture of 150 mg of $Pd(acac)_2$, 5 mL of benzyl alcohol and 30 mL of toluene at 30 °C for 1, 2, 3, or 7 days. Subsequently, the films were dried at room temperature for 1 day, and then annealed at 230 °C for 30 min under vacuum.

**2.4. TEM Observation.** The microdomain structures and the Pd nanoparticles in the annealed films were observed under a JEOL JEM-2000FX transmission electron microscope (TEM) operated at 200 kV for the ultrathin sections on the 100 mesh copper grids with formval supporting film. The ultrathin sections were prepared with a Leica EM FCS ultramicrotome equipped with a cryogenic sectioning kit at −75 °C and their thickness was about 70 nm. The ultrathin specimens of all the films before and after the reduction process were subjected to the TEM observation. All the TEM images were collected with a Bioscan CCD camera with 1k × 1k resolution.

**2.5. 3D Electron Tomography.** The ultrathin specimen after the reduction by immersing for 7 days and annealing in method 3 was subjected to single-axis electron tomography[47,50−53] to obtain the accurate sizes and the location of the nanoparticles in 3D space. The ultrathin specimen on the grid was tilted from −60° to +60° in 2° step in the TEM, and 61 images were obtained. For these images, we used the fiducial maker method using the reduced Pd nanoparticles as the markers to determine the tilt axis and to align the image positions. After the alignment we used the filtered back projection (FBP) method for 3D reconstruction.

**2.6. Particle Analysis.** *2.6.1. 2D Analysis.* We estimated the number and size of the particles in the TEM images by simply applying the image analyzing program for 2D images, using a freeware, ImageJ (http://rsb.info.nih.gov/ij/).

*2.6.2. 3D Analysis.* For the reconstructed 3D image obtained by 3D electron tomography, we measured the number and size of the particles directly from the 3D data set using Analyze 7.0 (visualization and analysis software: http://www.analyzedirect.com/). We measured the size of nanoparticles with the cross-section images of the 3D reconstruction instead of calculating directly from the particle volumes assuming a spherical shape of the nanoparticles because the 3D image of the nanoparticles are not perfectly spherical but more or less ellipsoidal due to the missing wedge effect. To avoid this problem, we extracted the largest value of the cross-sectional area of the nanoparticles images for each nanoparticle from a series of horizontal cross-sections of the 3D images.

**2.7. SAXS Measurements.** Small-angle X-ray scattering (SAXS) measurements were performed at room temperature to determine the morphology and the spacing of the nanostructures in the films of as-cast, after cross-linking with DIB, after immersion in the mixture solution for 3 days and after annealing at 230 °C using a SAXS instrument (RIGAKU, NANO-viewer) with an imaging plate (RIGAKU, R-AXISIV$^{++}$) as a detector. The SAXS profiles (intensity versus $q$, $q$: magnitude of wave vector) were obtained after correction for transmission and air scattering and circular averaging.

## 3. Results and Discussion

To control the location and the distribution of metal nanoparticles, it is necessary to modify their surface with protecting materials because the surfaces of the metal nanoparticles have high chemical potential and they easily aggregate together. In this work, we used PI-*b*-P2VP diblock copolymer because P2VP component helps the reduction of the Pd ion into Pd metal nanoparticles, and protects the Pd nanoparticles against their aggregation,[4−6] and the periodic microdomain structure of the block copolymer sustains these nanoparticles regularly and exclusively in the P2VP domains.

Figure 1 shows a TEM image of the thin section of PI-*b*-P2VP block copolymer film after cross-linking by DIB. The dark parts are P2VP domains with the contrast given by the

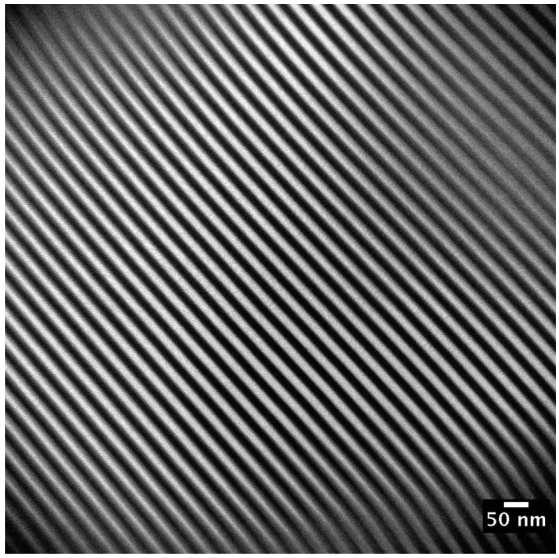


**Figure 1.** TEM image of the PI-*b*-P2VP film after cross-linking with DIB.

iodine atoms in the DIB cross-linking the P2VP chains, and bright parts are the PI domains. This TEM image shows that PI-*b*-P2VP maintains a lamellar morphology with a highly regular domain spacing of ca. 30 nm. This cross-linking treatment of P2VP domains is necessary to keep the lamellar microdomain structure during the subsequent immersion process. Without the cross-linking, the copolymer films are readily dissolved in the mixture solution. The cross-linked lamellar P2VP microdomains keep the entire film from dissolution because the lamellar microdomains are interconnected each other via Scherk's surfaces at the grain boundaries.[54]

**3.1. Method 1.** Figure 2a shows a TEM image of a thin section of the cross-linked PI-*b*-P2VP after immersing in the mixture solution of $Pd(acac)_2$, benzyl alcohol and toluene at 85 °C for 1 day. This treatment is similar to that employed by Adachi et al.[23] though we used benzyl alcohol instead of 1-propanol. In fact, we also tried exactly the same technique as theirs using 1-propanol but we found no Pd nanoparticles introduced in the bulk PI-*b*-P2VP film. Since 1-propanol is a poor solvent for PI and P2VP, we changed it to benzyl alcohol, which dissolves both PI and P2VP. In Figure 2a, some Pd nanoparticles have been generated sparsely both in PI and P2VP microdomains. It suggests that some $Pd(acac)_2$ and benzyl alcohol must have penetrated into the copolymer film during the immersion process and benzyl alcohol reduced $Pd(acac)_2$. At 85 °C benzyl alcohol works as a reduction agent for $Pd(acac)_2$, which can be deduced from the fact that after the immersing treatment, the color of the solution also turned into black due to the aggregated Pd nanoparticles. The reduction power of benzyl alcohol for $Pd(acac)_2$ is strong enough in solution at 85 °C. However, Figure 2a suggests either that not much $Pd(acac)_2$ and benzyl alcohol penetrated into the copolymer film or that not much reduction by benzyl alcohol proceeded in the copolymer film.

A breakthrough was made when we annealed the immersed films. Figure 2b shows a TEM image of a thin section of the PI-*b*-P2VP film after the solution-immersion treatment and subsequent annealing at 230 °C for 30 min in vacuum. The number of Pd nanoparticles increased dramatically after the annealing suggesting that immersion treatment introduced a large amount of $Pd(acac)_2$ into the copolymer film. The reduction of $Pd(acac)_2$ in the copolymer film must have proceeded in two steps, first by benzyl alcohol at 85 °C during the immersion treatment, and second by remaining benzyl alcohol in the dried film and/or P2VP itself when the film was subsequently annealed at 230 °C. By the reduction of $Pd(acac)_2$ during the immersion treatment, Pd nanoparticles were generated both in PI and P2VP domains although most of the Pd nanoparticles were generated predominantly in the P2VP microdomains during the annealing process. Therefore, the selectivity of the introduction of Pd nanoparticles into the P2VP domains in method 1 is good to some extent but not perfect. To achieve a higher selectivity we need to avoid the generation of Pd nanoparticles during the immersion process in the mixture solution.

**3.2. Method 2.** The reduction of $Pd(acac)_2$ in the annealing process at 230 °C is considered to be promoted predominantly by P2VP within the P2VP domains but not by benzyl alcohol. Therefore, to achieve a higher selectivity it is necessary to avoid the generation of Pd nanoparticles in the PI domains during the immersing process in the mixture solution. If the role of benzyl alcohol is just to reduce the Pd ion and P2VP can reduce the Pd ion better than benzyl alcohol at 230 °C, benzyl alcohol is not necessary. We immersed the PI-*b*-P2VP film cross-linked with DIB into the mixture solution without benzyl alcohol at two different temperatures, 30 and 85 °C. The yellowish color of the mixture solution was unchanged even after the immersion treatments at both temperatures, suggesting that no reduction of $Pd(acac)_2$ took place in the mixture solution. We confirmed no generation of Pd nanoparticles in the polymer films at this step as well by TEM observation. Subsequently, the films were annealed at 230 °C for 30 min under vacuum. Figure 3 shows the TEM images of the specimens annealed after immersion at 30 °C (Figure 3a) and 85 °C (Figure 3b). In Figure 3b we can find only one Pd nanoparticle in the PI microdomains as pointed by an arrow. The selectivity in the generation of Pd nanoparticles in the P2VP microdomains in method 2 is much higher than method 1. However, the number of Pd nanoparticles generated after the annealing in method 2 is much less than method 1. This could be attributed to the absence of benzyl alcohol in the mixture solution, which is the only difference between method 1 and method 2 in case of immersion temperature of 85 °C. We suspect that benzyl alcohol must have promoted the penetration of Pd ion into the P2VP domains. Since toluene is a relatively poor solvent for P2VP and, moreover, since the P2VP domains were cross-linked by DIB, the mixture solution and, therefore, the Pd ion scarcely penetrate into the P2VP domains without the assistance of benzyl alcohol as observed in method 2. As the result, only a very small amount of Pd ion was introduced into the P2VP domains during the immersion process in the mixture solution in method 2, and a very small number of Pd nanoparticles were generated during annealing at 230 °C. The significant difference in the amount of the introduced Pd nanoparticles between method 1 and method 2 indicates that benzyl alcohol is necessary to increase the amount of Pd nanoparticles introduced in the P2VP domains. Thus, benzyl alcohol is necessary ingredient to introduce Pd ion into the P2VP domains by selectively swelling them since benzyl alcohol is a good solvent for both P2VP and $Pd(acac)_2$.

**3.3. Method 3.** Instead of removing benzyl alcohol as we did in method 2, we chose a different approach in method 3. To avoid the reduction of the $Pd(acac)_2$ by benzyl alcohol in the mixture solution as well as in the cross-linked film during the immersion process, we immersed the cross-linked polymer films in the mixture solution at 30 °C for different periods of time, dried them in the ambient atmosphere, and then annealed at 230 °C for 30 min in vacuum. At 30 °C the yellowish color of the mixture solution was unchanged after the immersion process and $Pd(acac)_2$ in the solution was not reduced by benzyl alcohol.

We confirmed by TEM observation that no Pd nanoparticle was generated in the polymer films after the immersion process

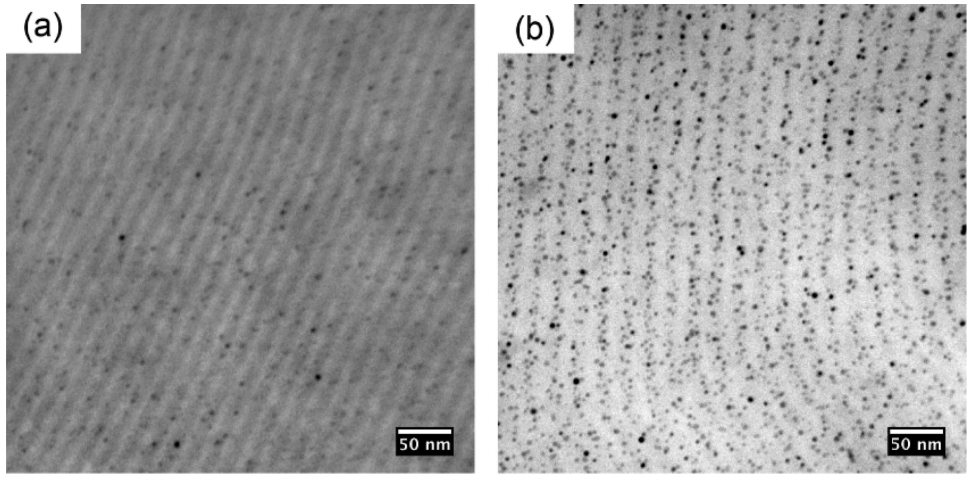


**Figure 2.** TEM images of the PI-*b*-P2VP films (a) after immersion in the mixture solution containing benzyl alcohol for 1 day at 85 °C, and (b) after subsequent annealing at 230 °C for 30 min (method 1).

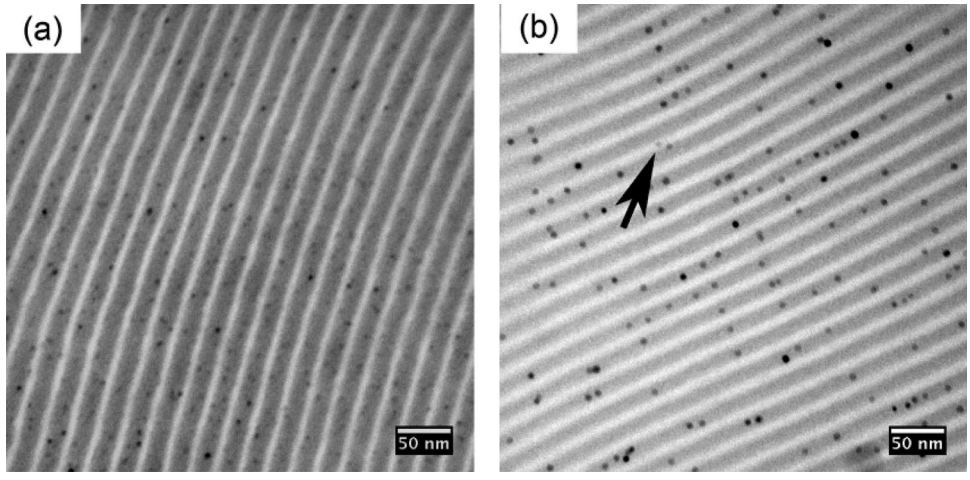


**Figure 3.** TEM images of the PI-*b*-P2VP films after immersion in the mixture solution without benzyl alcohol for 1 day at (a) 30 °C and (b) 85 °C, and subsequently annealed at 230 °C for 30 min (method 2).

and that the lamellar structure was not disturbed by the immersion process in the mixture solution in method 3. This suggests that the immersing treatment at a temperature as low as 30 °C does not alter the original lamellar morphology in the cross-linked film nor generate Pd nanoparticles even though the mixture solution contains benzyl alcohol. After the immersion for 1−7 days, the polymer films were dried and annealed at 230 °C for 30 min in vacuum. Figure 4 shows the TEM images after annealing for the immersion time of (a) 1 day, (b) 2 days, (c) 3 days, and (d) 7 days. All TEM images in Figure 4 exhibit the high selectivity in the introduction of Pd nanoparticles into the P2VP microdomains. Comparing all the TEM images in Figure 4, we noticed that the number of Pd nanoparticles increased with the immersion time while the dark contrast of the P2VP domains decreased. Though the contrast in the TEM images is always relative and absolute concentration of DIB cannot be judged by the darkness alone in the TEM images, the reduction of darkness in the P2VP microdomains with the immersion time exceeds the level of darkness change with contrast manipulation taking the Pd nanoparticle image as the standard. Then, it suggests that the P2VP chains cross-linked by DIB must have released a portion of the DIB when annealed at 230 °C and this release must be related to the reduction mechanism of the Pd ion penetrated into the P2VP domains. As the result, Pd nanoparticles were generated only in the P2VP domains in the reduction process. In addition, because the sublimation temperature of $Pd(acac)_2$ is 170 °C, which is lower than the annealing temperature, 230 °C, the remaining intact $Pd(acac)_2$ in the P2VP microdomains as well as those in the PI microdomains, which did not make the complex with the P2VP chains, sublimed during the annealing process under the reduced pressure. The released DIB must have been removed from the film at the same time. It should be noted, however, that the copolymer films with the Pd nanoparticles after the annealing could not be dissolved in toluene due to either the cross-links between the remaining DIB and the P2VP chains or the adhesion between the Pd nanoparticles and the P2VP chains. Thus, we could establish the technique of in situ introduction of Pd nanoparticles selectively into the P2VP microdomains of PI-*b*-P2VP diblock copolymer. Cross-linking with DIB helped not only keeping the microdomain structure unchanged during the immersion and annealing processes, but also avoiding the dissolution of the film in the mixture solution, and achieving the highly selective introduction of Pd nanoparticles into the P2VP domains, which will be demonstrated by 3D electron tomography below.

**3.4. Particle Analysis.** The number of Pd nanoparticles per unit area and their average size were measured as a function of immersion time in the mixture solution for method 3 using the TEM images of the films after annealing with the aid of an image processing software ImageJ. The results are plotted in Figure 5. It shows the tendency of the average size of the Pd nanoparticles increasing with the immersion time. But the

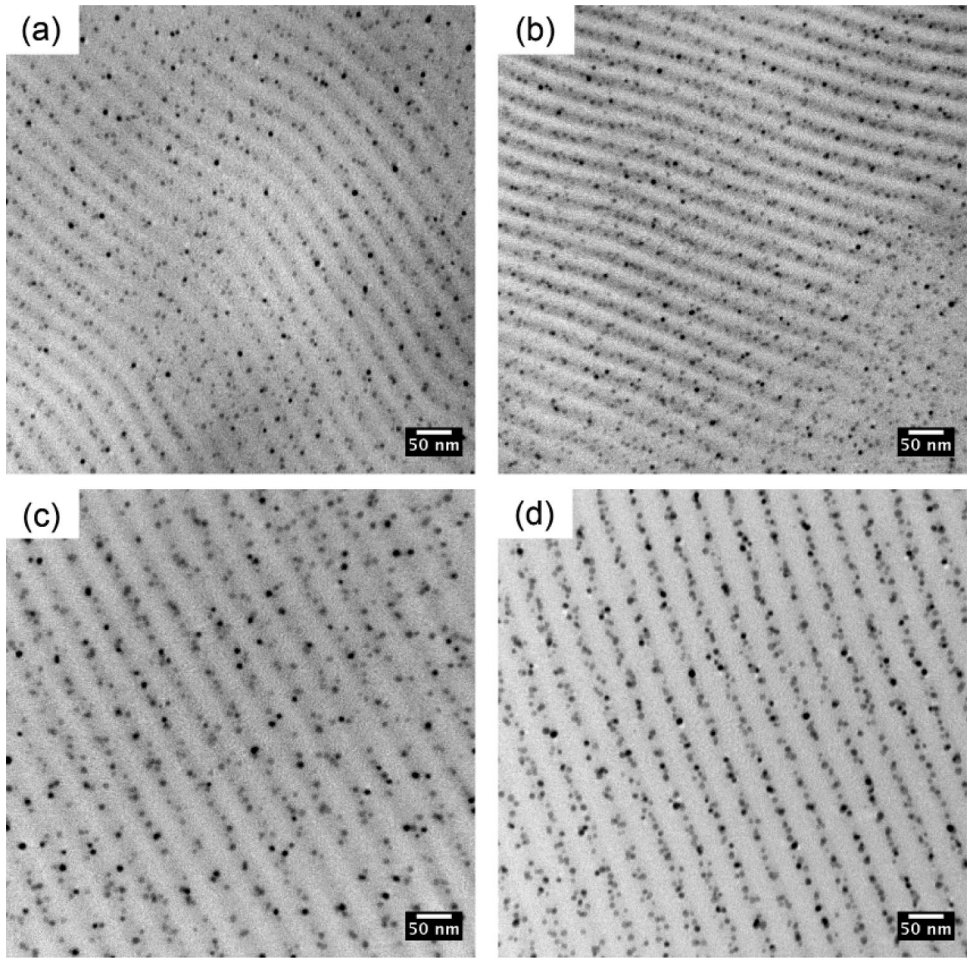


**Figure 4.** TEM images of the cross-linked PI-*b*-P2VP films after immersion in the mixture solution with benzyl alcohol at 30 °C for (a) 1 day, (b) 2 days, (c) 3 days, and (d) 7 days, and subsequently annealed at 230 °C for 30 min. (method 3).

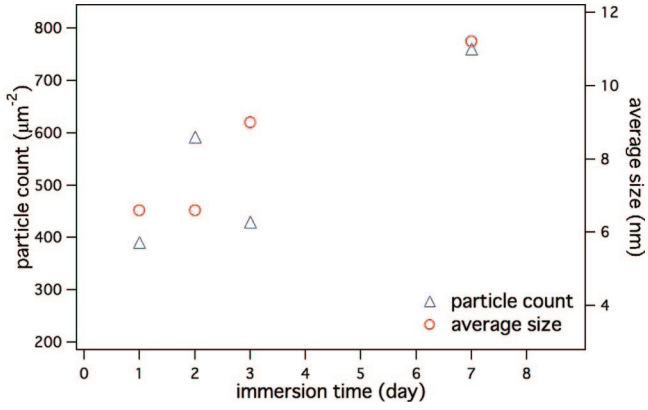


**Figure 5.** Result of the 2D analysis of the TEM images of the PI-*b*-P2VP films by method 3 with ImageJ. The number of the Pd nanoparticles per unit area ($\mu m^{-2}$) and their average size are plotted against the immersion time.

increase in the number of Pd nanoparticles per unit area is not straightforward with time. We suspected that this irregularity is resulted from the error in identifying individual particles in the TEM images using the image analysis procedure of the software. Since TEM images are the 2D projections of the 3D objects, it is impossible to separate individual particles from each other if the images of more than two particles overlapped in the thickness direction of the thin sections, resulting in measuring the size of the "aggregate" of more than two particles as that of a single particle. Then, what we can get are the wrong number and size of the particles. To avoid this problem, we applied the 3D electron tomography technique to the particle analysis in 3D space.

Figure 6 shows the 3D reconstructed image obtained from the same area as shown in Figure 4d for the film immersed for 7 days. The volume size of the 3D reconstructed image is 400 nm × 400 nm × 100 nm. The Pd nanoparticles belonging to different P2VP lamellar domains are shown in different colors. All the Pd nanoparticles seem to be located within each P2VP domain. By observing the 3D image rotating around the vertical axis, we found that the distribution of the Pd nanoparticles with respect to the lamellar center was much sharper than it appeared in Figure 6. All the individual Pd nanoparticles can be separated in this measurement and thus it involved no error due to the overlapping of the Pd nanoparticles. This also shows that the generation of the Pd nanoparticles was limited within the P2VP microdomains. We measured the number and the size of the Pd nanoparticles from the 3D reconstructed image. The number of the Pd nanoparticles turned out to be 779 in the volume of $1.6 \times 10^6$ nm$^3$ and their average size was 5.5 nm. In the 2D particle analysis for the same area, the number of the Pd nanoparticles was 207 and their average size was 9.2 nm. This suggests clearly that the number of the Pd nanoparticles was underestimated due to their overlapping in the projected TEM image. Therefore, 2D particle analysis is not an accurate method to measure the number and the size of nanoparticles excepting the case where all the particles are sparsely distributed. We applied 3D electron tomography to each of the four samples observed in Figure 4, and measured the number and the size of the Pd nanoparticles. Figure 7 shows the average size and the

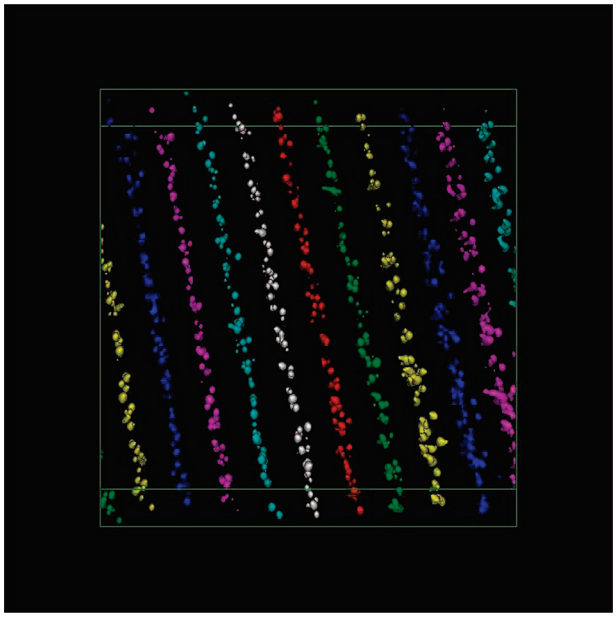

**Figure 6.** 3D electron tomography image reconstructed for the same area as shown in Figure 5d for the PI-*b*-P2VP film immersed for 7 days in the mixture solution with benzyl alcohol in method 3. Pd nanoparticles in each P2VP lamellar domain are distinguished by different colors (volume size: 400 nm × 400 nm × 100 nm).

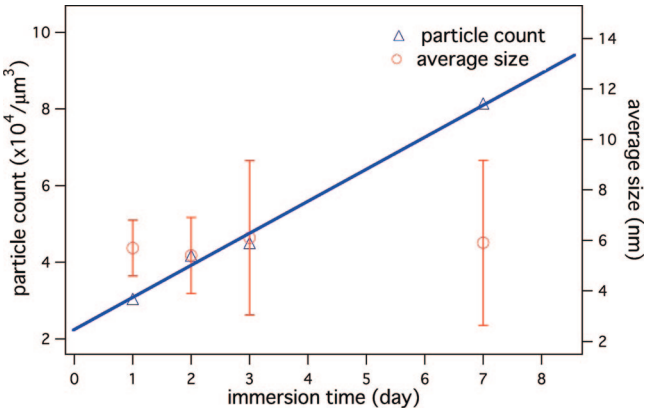


**Figure 7.** Result of the 3D analysis of the TEM images of the PI-*b*-P2VP films by method 3 with Analyze7.0. The number of the Pd nanoparticles per unit volume ($\mu m^{-3}$) and their average size are plotted against the immersion time.

number of the Pd nanoparticles vs immersion time in the mixture solution. It shows that the average size of the Pd nanoparticles is almost independent of immersion time in contrast to the increasing tendency for the 2D analysis in Figure 5. Therefore, we can conclude that the size of the Pd nanoparticles does not depend on the immersion time. However, the number of the Pd nanoparicles increased almost linearly with the immersion time as shown by the solid line in Figure 7.

Figure 8 shows the size distribution of the nanoparticles obtained by each method. The data with annotation "3D" represent the distribution obtained by the 3D particle analysis, and the others by the 2D particle analysis. Here $C_r$ and $C_0$ represent the count of the Pd nanoparticles having a particular size and the total count of the Pd nanoparticles in the image, respectively. The distribution curves obtained by the 2D particle analysis for method 1, method 2 at 30 °C and method 2 at 85 °C are considerably sharp and their average sizes are 4.5, 3.6, and 5.2 nm, respectively. However, the selectivity of introduction for method 1 is not so good, and the total count of the Pd nanoparticles for method 2 is very small. When we compare

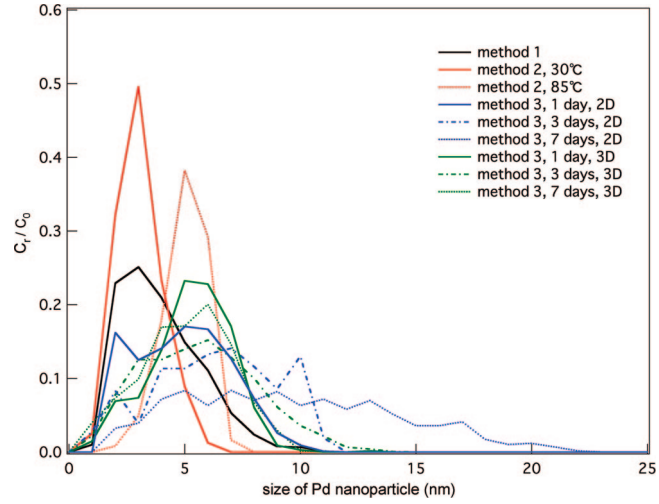


**Figure 8.** Size distribution of the Pd nanoparticles obtained by each method. $C_r$ and $C_0$ represent the count of the Pd nanoparticles having a particular size and the total count of Pd nanoparticles, respectively.

the distribution curves obtained by the 3D particle analysis with that of the 2D particle analysis for method 3, we notice that the curves obtained by the 2D particle analysis for the immersion of 3 and 7 days have a significant count of larger nanoparticles due to the overlapping of the several Pd nanoparticles in the projected TEM images. The distribution curves obtained by the 3D image analysis are more accurate because all Pd nanoparticles in the 3D reconstructed image are distinguishable from each other and counted or measured. Overlapping of Pd nanoparticles in the projected TEM image in the 2D analysis leads to an incorrect result both in their count and their sizes. This tendency increases with an increase in the number density of Pd nanoparticles. In contrast, the particle analysis for the TEM images with smaller number density of Pd nanoparticles and hence with isolated Pd nanoparticles does not have such a problem.

Since we attempted to introduce the Pd nanoparticles uniformly into the bulk film, we needed to examine the distribution of the Pd nanoparticle concentration across the film thickness. Nonuniform introduction of nanoparticles across the film thickness is unfavorable for a practical application in many cases. Therefore, we applied electron tomography to several different areas as a function of the depth from the surface for the PI-*b*-P2VP film prepared by method 3 with the immersion time of 7 days. Figure 9 shows the low magnification TEM image of the same specimen as observed for Figure 4d. The TEM image in Figure 9 shows the area from the surface to the interior of the bulk film specimen after the introduction of the Pd nanoparticles. The black line on the TEM image indicates the location of the surface of the bulk film. The areas where the electron tomography was performed are designated by the dots marked with a−d. The electron tomography of the area near the center of the bulk film (250 $\mu$m from the surface) was performed with a different thin section. Figure 10 shows the average size (open circles) and the number (open triangles) of the Pd nanoparticles as a function of the distance from the surface of the bulk film. The average size of the Pd nanoparticles is kept almost constant independent of the depth from the film surface, and so is the number of the Pd nanoparticles per unit volume except for the area very close to the surface of the bulk film where the concentration of the Pd nanoparticle is 2−3 times higher than that in the interior. Probably a higher concentration of Pd ion near the film surface gave rise to the higher concentration of Pd nanoparticles near the film surface. Thus we could achieve a fairly uniform introduction of Pd nanopar-

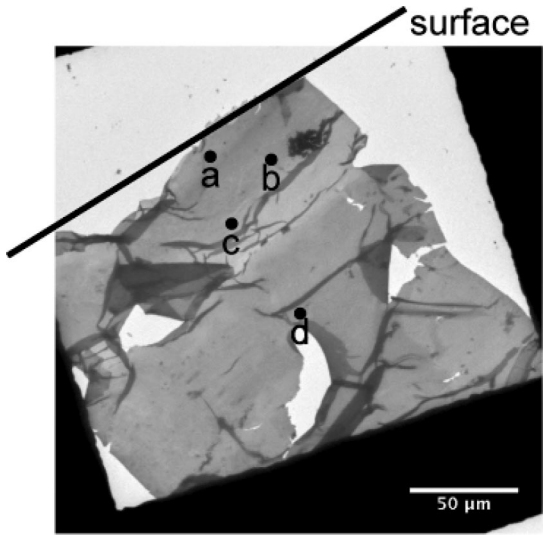


**Figure 9.** Low magnification TEM image of the ultrathin section of the PI-*b*-P2VP film immersed for 7 days and annealed exposing the cross-section including the film surface. The dark areas correspond to the grid bars and the solid line indicates the location of film surface.

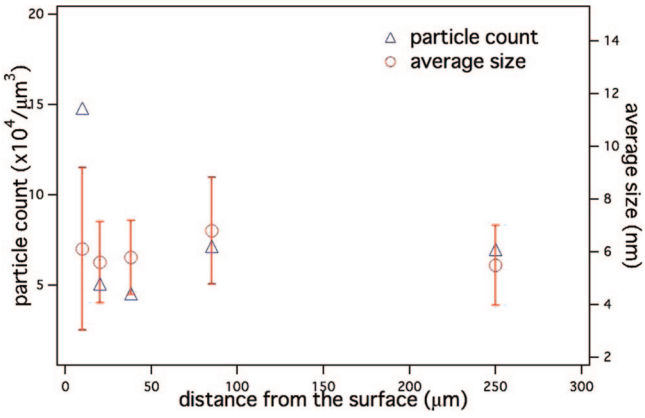


**Figure 10.** Result of the 3D analysis of the TEM images of the PI-*b*-P2VP films by method 3 with Analyze7.0. The number of the Pd nanoparticles per unit volume ($\mu m^{-3}$) and their average size are plotted against the distance from the surface of the bulk film.

ticles across the film thickness except for the very narrow region from the surface. Immersion of the cross-linked PI-*b*-P2VP in the mixture solution for 7 days in method 3 seems to be long enough to achieve uniform distribution of Pd ion in the bulk film specimen.

**3.5. SAXS Analysis.** The domain spacing of the microdomain structure for each step of the processing of the copolymer film immersed for 3 days in method 3 were measured by SAXS experiments, and the average size of the Pd nanoparticles produced in the final step was also calculated. Figure 11 shows the SAXS profiles of the films of as-cast (open circles), after cross-linking with DIB (crosses), after immersion for 3 days (open squares), and after annealing at 230 °C (open triangles), respectively. Here, $q$ and $I(q)$ represent magnitude of scattering vector and scattering intensity at $q$, respectively. All the SAXS profiles suggest lamellar structure because the higher-order peaks appear at the $q$ positions of integer multiples of the $q$ value at each first-order peak. The film after cross-linking exhibits up to the 10th-order peak suggesting a highly regular spacing of the lamellae. The domain spacing and the thickness of each microdomain were evaluated from the SAXS profiles by their self-correlation function

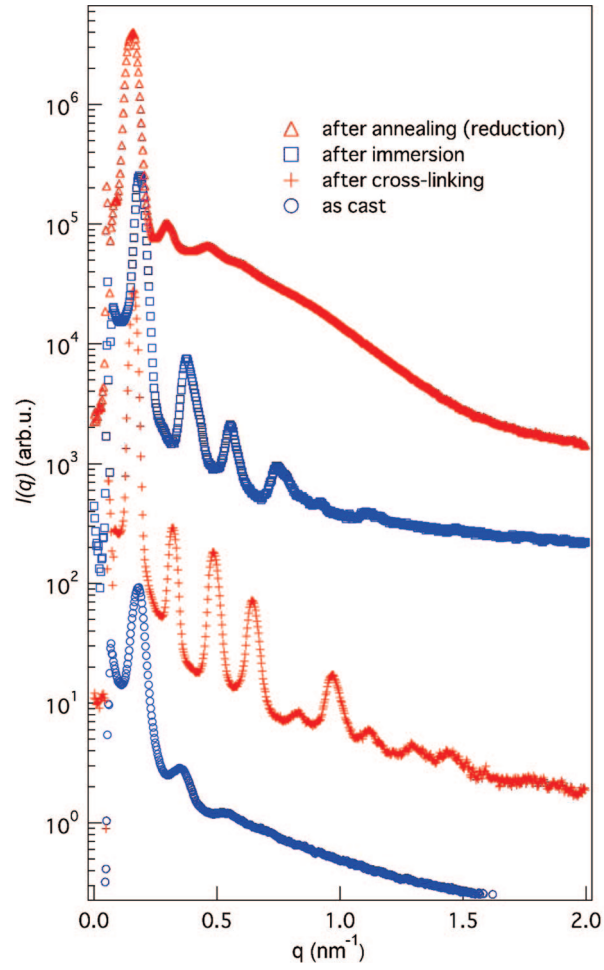


**Figure 11.** SAXS profile from the film as cast, after cross-linking with DIB, after immersion for 3 days, and after annealing at 230 °C. All the profiles indicate lamellae morphology.

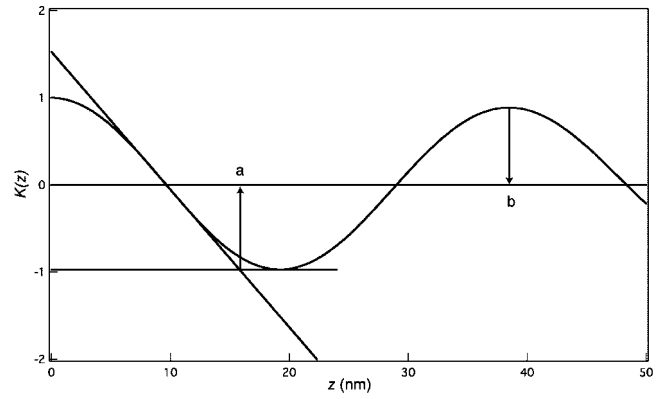


**Figure 12.** Self-correlation function $K(z)$ vs distance $z$ plot for the SAXS profile of the film after cross-linking with DIB in method 3 (immersion time: 3 days). The distances marked by $a$ and $b$ correspond to the thickness of the P2VP microdomain and the domain spacing, respectively.

described by eq 1. Here $K(z)$ and $z$ represent self-correlation function and distance, respectively.

$$K(z) = \frac{\int 4\pi q^2 I(q) \cos qz \, dq}{\int 4\pi q^2 I(q) \, dq} \quad (1)$$

In Figure 12, $K(z)$ is plotted against $z$ for the SAXS profile of the cross-linked film. The points $a$ and $b$ correspond to the

**Table 1. Domain Spacing, and the Thicknesses of P2VP and PI Domains Determined from $K(z)$ and $z$ Obtained from the SAXS Profiles**

| | $b$ (domain spacing) (nm) | $a$ (thickness of P2VP microdomain) (nm) | $b - a$ (thickness of PI microdomain) (nm) |
|---|---|---|---|
| as cast | 33.3 | 13.2 | 20.1 |
| after cross-linking | 38.5 | 15.7 | 22.8 |
| after immersion | 32.8 | 13.3 | 19.5 |
| after annealing | 38.5 | 15.4 | 23.1 |

thickness of the P2VP microdomain and the domain spacing, respectively, so the thickness of the PI microdomain is given by $(b - a)$. Similarly, the domain spacing and the thicknesses of the PI and P2VP microdomains of the other three films were obtained and listed in Table 1. The domain spacings of the films after cross-linking with DIB and after annealing at 230 °C are the same and larger than the others. Table 1 also shows that the thicknesses of both PI and P2VP microdomains of the films after cross-linking and after annealing at 230 °C are thicker than the others. This suggests that the increase in the thickness of each microdomain after annealing at 230 °C or after cross-linking by exposing to DIB vapor at 85 °C could be the result of thermal equilibration by heating, but was not caused by the addition of the DIB, Pd ion or Pd nanoparticles into the microdomains. On the other hand, the as-cast film and the film after immersion in the mixture solution have smaller domain spacings and thicknesses of the PI and P2VP microdomains than the others because of the nonequilibrium states frozen-in after the evaporation of solvents at room temperature. The thermal treatment above the glass transition temperature of P2VP or solvent annealing with DIB at 85 °C promoted the molecular motion to attain the equilibrium states and brought an increase in the thickness of each microdomain. Consequently, we could confirm that the lamellar microdomain structure of PI-*b*-P2VP was not disturbed at all by each processing step in method 3.

The SAXS profile after annealing at 230 °C as shown in Figure 11 is composed of the scattering from the microdomain structure (sharp peaks) and that from the Pd nanoparticles (broad shoulder). Assuming that the Pd nanoparticles are spherical and their distribution has no correlation, the scattering intensity $I_p(q)$ is approximately expressed by

$$I_p(q) = CN\int_0^\infty P(R)\left[\frac{4\pi R^3}{3}\Phi(qR)\right]^2 \mathrm{d}R \tag{2}$$

$$\Phi(qR) = \frac{3}{(qR)^3}[\sin(qR) - (qR)\cos(qR)] \tag{3}$$

Here $R$ is the radius of spherical particles, $N$ is the total number of particles, $P(R)$ is a distribution function describing the number of particles having a radius $R$, and $C$ is a constant independent of $q$ and $R$. In Figure 13, the solid line shows the best-fitted curve of $I_p(q)$ obtained by eq 2 when $P(R)$ is approximated by the Gaussian distribution and $R = 2.9$ nm, and the dashed line shows the best-fitted curve when there is no distribution in $R$ and $R = 2.9$ nm to the SAXS profile of after annealing at 230 °C shown by open circles. The diameter of Pd nanoparticles obtained by SAXS experiment, 5.8 nm is in good agreement with that obtained by 3D electron tomography, 6.1 nm, within the experimental error.

## 4. Conclusion

We successfully developed the technique to control the introduction of Pd nanoparticles with an extremely high selectivity into the P2VP domains of the PI-*b*-P2VP diblock copolymer, as well as to control the number of introduced Pd nanoparticles. The technique consists of three steps: (i) cross-linking of P2VP domains of PI-*b*-P2VP film with DIB, (ii) immersion of the cross-linked film in the mixture of $Pd(acac)_2$, benzyl alcohol and toluene at 30 °C, and (iii) annealing the immersed film at 230 °C for 30 min. The new issue of this study is the introduction of Pd ions and the generation of Pd nanoparticles in situ in the P2VP domains fixed by cross-linking of P2VP with DIB, which prevents the dissolution of polymer films in the mixture solutions, so that there is no significant change of the microdomain structure even after the introduction of Pd nanoparticles. Pd nanoparticles with a relatively uniform size can be uniformly introduced in the bulk film of 0.5 mm thick.

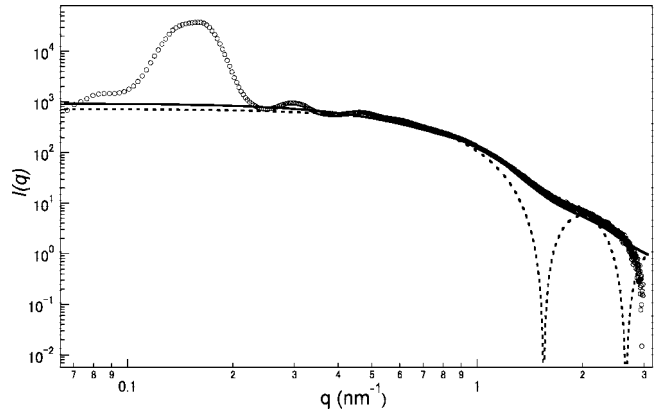


**Figure 13.** The curve-fitting results using eqs 2 and 3 with the SAXS profile of the film obtained by method 3 (immersion time: 3 days). The dashed and solid curves are the best-fitted curves for the spherical particles with 5.8 nm diameter without size distribution and with Gaussian distribution, respectively.

We also applied 3D electron tomography to analyze the location and the size of the Pd nanoparticles in 3D real space. Consequently, we could show the significant difference between the 2D and the 3D analyses. The electron tomography is a powerful tool to analyze the nanoparticle/block copolymer systems in real space. Furthermore, we examined the thickness of the lamellar microdomains and the size of the Pd nanoparticles by SAXS. As the result, we could prove that the lamellar microdomain structure of PI-*b*-P2VP did not undergo a significant change throughout the treatment processes. A good agreement was confirmed between the size measurements of the Pd nanoparticles by electron tomography and SAXS.

**Acknowledgment.** The authors thank Naoki Sakamoto, Asahi KASEI Co., for his technical support on the SAXS analysis. This work was supported in part by a Grant-in-Aid for Scientific Research (under Grant No. 17105004(S)) from the Japan Society for the Promotion of Science (JSPS).

## References and Notes

(1) Woratschek, B.; Ertl, G.; Kuppers, J.; Sesselmann, W.; Haberland, H. *Phys. Rev. Lett.* **1986**, *57*, 1484–1487.
(2) Hodes, G.; Albuyaron, A.; Decker, F.; Motisuke, P. *Phys. Rev. B* **1987**, *36*, 4215–4221.
(3) Otero, R.; de Parga, A. L. V.; Miranda, R. *Phys. Rev. B* **2002**, *66*, 115401.
(4) Toshima, N.; Takahashi, T. *Bull. Chem. Soc. Jpn.* **1992**, *65*, 400–409.
(5) Brust, M.; Walker, M.; Bethell, D.; Schiffrin, D. J.; Whyman, R. *J. Chem. Soc., Chem. Commun.* **1994**, (7), 801–802.
(6) Pileni, M. P. *Langmuir* **1997**, *13*, 3266–3276.
(7) Mayer, A. B. R.; Mark, J. E. *Colloid Polym. Sci.* **1997**, *275* (4), 333–340.
(8) Bronstein, L. M.; Chernyshov, D. M.; Timofeeva, G. I.; Dubrovina, L. V.; Valetsky, P. M.; Khokhlov, A. R. *J. Colloid Interface Sci.* **2000**, *230* (1), 140–149.
(9) Lopes, W. A. *Phys. Rev. E* **2002**, *65*, 031606.
(10) Sadron, C.; Gallot, B. *Makromol. Chem.—Macromol. Chem. Phys.* **1973**, *164*, 301–332.

(11) Hashimoto, T.; Shibayama, M.; Fujimura, M.; Kawai, H.; Meier D. J. Ed.; *Block Copolymer Science and Technology*; MMI Press/Harwood Academic: New York, 1983; p 63.
(12) Thomas, E. L.; Alward, D. B.; Kinning, D. J.; Martin, D. C.; Handlin, D. L.; Fetters, L. J. *Macromolecules* **1986**, *19*, 2197–2202.
(13) Hasegawa, H.; Tanaka, H.; Yamasaki, K.; Hashimoto, T. *Macromolecules* **1987**, *20*, 1651–1662.
(14) Hajduk, D. A.; Harper, P. E.; Gruner, S. M.; Honeker, C. C.; Kim, G.; Thomas, E. L.; Fetters, L. J. *Macromolecules* **1994**, *27*, 4063–4075.
(15) Hamley, I. *The Physics of Block Copolymers*; Oxford Univ. Press: Oxford, U.K., 1988.
(16) Mayer, A. B. R. *Mater. Sci. Eng. C: Biomimetic Supramol. Syst.* **1998**, *6* (2−3), 155–166.
(17) Haryono, A.; Binder, W. H. *Small* **2006**, *2*, 600–611.
(18) Hashimoto, T.; Harada, M.; Sakamoto, N. *Macromolecules* **1999**, *32*, 6867–6870.
(19) Tsutsumi, K.; Funaki, Y.; Hirokawa, Y.; Hashimoto, T. *Langmuir* **1999**, *15*, 5200–5203.
(20) Ribbe, A. E.; Okumura, A.; Matsushige, K.; Hashimoto, T. *Macromolecules* **2001**, *34*, 8239–8245.
(21) Hashimoto, T.; Okamura, A.; Tanabe, D. *Macromolecules* **2003**, *36*, 7324–7330.
(22) Horiuchi, S.; Fujita, T.; Hayakawa, T.; Nakao, Y. *Langmuir* **2003**, *19*, 2963–2973.
(23) Adachi, M.; Okumura, A.; Sivaniah, E.; Hashimoto, T. *Macromolecules* **2006**, *39*, 7352–7357.
(24) Lee, D.; Rubner, M. F.; Cohen, R. E. *Chem. Mater.* **2005**, *17*, 1099–1105.
(25) Zehner, R. W.; Sita, L. R. *Langmuir* **1999**, *15*, 6139–6141.
(26) Tanaka, H.; Koizumi, S.; Hashimoto, T.; Itoh, H.; Satoh, M.; Naka, K.; Chujo, Y. *Macromolecules* **2007**, *40*, 4327–4337.
(27) Semagina, N. V.; Bykov, A. V.; Sulman, E. M.; Matveeva, V. G.; Sidorov, S. N.; Dubrovina, L. V.; Valetsky, P. M.; Kiselyova, O. I.; Khokhlov, A. R.; Stein, B.; Bronstein, L. M. *J. Mol. Catal. a: Chem.* **2004**, *208* (1−2), 273–284.
(28) Bockstaller, M.; Kolb, R.; Thomas, E. L. *Adv. Mater.* **2001**, *13*, 1783–1786.
(29) Morkved, T. L.; Wiltzius, P.; Jaeger, H. M.; Grier, D. G.; Witten, T. A. *Appl. Phys. Lett.* **1994**, *64*, 422–424.
(30) Zehner, R. W.; Lopes, W. A.; Morkved, T. L.; Jaeger, H.; Sita, L. R. *Langmuir* **1998**, *14*, 241–244.
(31) Lin, B. H.; Morkved, T. L.; Meron, M.; Huang, Z. Q.; Viccaro, P. J.; Jaeger, H. M.; Williams, S. M.; Schlossman, M. L. *J. Appl. Phys.* **1999**, *85*, 3180–3184.
(32) Sohn, B. H.; Seo, B. W.; Yoo, S. I. *J. Mater. Chem.* **2002**, *12*, 1730–1734.
(33) Lopes, W. A.; Jaeger, H. M. *Nature* **2001**, *414* (6865), 735–738.
(34) Bockstaller, M. R.; Lapetnikov, Y.; Margel, S.; Thomas, E. L. *J. Am. Chem. Soc.* **2003**, *125*, 5276–5277.
(35) Spatz, J. P.; Mossmer, S.; Hartmann, C.; Moller, M.; Herzog, T.; Krieger, M.; Boyen, H. G.; Ziemann, P.; Kabius, B. *Langmuir* **2000**, *16*, 407–415.
(36) Spatz, J. P.; Roescher, A.; Moller, M. *Adv. Mater.* **1996**, *8*, 337–340.
(37) Kim, Y. W.; Lee, D. K.; Lee, K. J.; Min, B. R.; Kim, J. H. *J. Polym. Sci., Part B: Polym. Phys.* **2007**, *45*, 1283–1290.
(38) Boontongkong, Y.; Cohen, R. E. *Macromolecules* **2002**, *35*, 3647–3652.
(39) Joly, S.; Kane, R.; Radzilowski, L.; Wang, T.; Wu, A.; Cohen, R. E.; Thomas, E. L.; Rubner, M. F. *Langmuir* **2000**, *16*, 1354–1359.
(40) Coffee, S. S.; Stanley, S. K.; Ekerdt, J. G. *J. Vacuum Sci. Technol. B* **2006**, *24*, 1913–1917.
(41) Bronstein, L. H.; Sidorov, S. N.; Valetsky, P. M.; Hartmann, J.; Colfen, H.; Antonietti, M. *Langmuir* **1999**, *15*, 6256–6262.
(42) Tadd, E. H.; Bradley, J.; Tannenbaum, R. *Langmuir* **2002**, *18*, 2378–2384.
(43) Harris, L. A.; Goff, J. D.; Carmichael, A. Y.; Riffle, J. S.; Harburn, J. J.; St Pierre, T. G.; Saunders, M. *Chem. Mater.* **2003**, *15*, 1367–1377.
(44) Huh, J.; Ginzburg, V. V.; Balazs, A. C. *Macromolecules* **2000**, *33*, 8085–8096.
(45) Thompson, R. B.; Ginzburg, V. V.; Matsen, M. W.; Balazs, A. C. *Science* **2001**, *292* (5526), 2469–2472.
(46) Lee, J. Y.; Thompson, R. B.; Jasnow, D.; Balazs, A. C. *Phys. Rev. Lett.* **2002**, *89*, 155503.
(47) Jinnai, H.; Kaneko, T.; Nishioka, H.; Hasegawa, H.; Nishi, T. *Chem. Record* **2006**, *6* (5), 267–274.
(48) Kim, B. J.; Chiu, J. J.; Yi, G. R.; Pine, D. J.; Kramer, E. J. *Adv. Mater.* **2005**, *17*, 2618–2622.
(49) Deshmukh, R. D.; Liu, Y.; Composto, R. J. *Nano Lett.* **2007**, *7*, 3662–3668.
(50) Frank, J. *Electron Tomography*; 2nd ed., Springer-Verlag: New York, 2006.
(51) Koster, A. J.; Grimm, R.; Typke, D.; Hegerl, R.; Stoschek, A.; Walz, J.; Baumeister, W. *J. Struct. Biol.* **1997**, *120*, 276–308.
(52) Dohi, H.; Kimura, H.; Kotani, M.; Kaneko, T.; Kitaoka, T.; Nishi, T.; Jinnai, H. *Polym. J.* **2007**, *39*, 749–758.
(53) Mareau, V. H.; Akasaka, S.; Osaka, T.; Hasegawa, H. *Macromolecules* **2007**, *40*, 9032–9039.
(54) Nishikawa, Y.; Kawada, H.; Hasegawa, H.; Hashimoto, T. *Acta Polym.* **1993**, *44* (5), 247–255.

MA802674K